Available online at www.sciencedirect.com

ScienceDirect

Journal of Magnesium and Alloys 10 (2022) 449–457

www.elsevier.com/locate/jma

Full Length Article

Experimental measurement on the phase equilibria of the Mg–Ag–Cu ternary system at 350 and 400 °C

Jian Wang[a,b,*], Zhang Zhang[a,b], Yinju Zhang[a], Liling Jin[c], Liyuan Sheng[b,*]

[a] College of Mechanical Engineering, Yangzhou University, Yangzhou 225127, China
[b] Shenzhen Institute, Peking University, Shenzhen 518057, Guangdong Province, China
[c] Center for Research in Computational Thermochemistry (CRCT), Department of Chemical Engineering, Ecole polytechnique de Montréal, Montréal H3C 3A7, Québec, Canada

Received 13 April 2020; received in revised form 2 June 2020; accepted 14 December 2020
Available online 16 February 2021

Abstract

The phase equilibria of the Mg–Ag–Cu ternary system at 350 and 400 °C were experimentally investigated using twenty-eight key samples. The phase equilibria and compositions in key samples were investigated using scanning electron microscopy (SEM) equipped with energy-dispersive spectroscopy (EDS). Powder X-ray diffraction (XRD) technique was used to analyze the crystal structure and solid solubility of compounds. Five three-phase equilibria and several two-phase equilibria have been determined at 350 and 400 °C. The solid solubility range of Cu in the compounds Mg_3Ag, MgAg and fcc(Ag) were examined at 350 and 400 °C. The maximum solid solubility of Ag in the compound $MgCu_2$ was found to be 11.46 at.% and 11.25 at.% with a constant value of about 66 at.% Cu at 350 and 400 °C, respectively. Besides, the solid solubility limits of Ag in the compounds Mg_2Cu and fcc(Cu) were found to be less than 5 at.% at 350 and 400 °C. No ternary compound was observed in the present work.

Keywords: Mg–Ag–Cu system; Phase diagram; SEM; EDS; XRD.

1. Introduction

Permanent implants used for bone repairing often have biocompatibility problems and ordinary inflammatory response. Physical pain and financial burden are the main disadvantages of secondary surgery for the removal of permanent implants [1]. To this end, biodegradable implants become one of the great exciting research topics. As metal materials, magnesium, with a density and elastic modulus close to human skeleton, can effectively reduce the stress shielding effect [2]. Therefore, magnesium alloys could be the new generation of biomaterials because of their excellent properties of biocompatibility and biodegradability [3,4]. The main problem of the magnesium alloy as degradable implants is that its degradation rate is too fast, which leads to the premature failure of implants. The prerequisite of magnesium alloys as biodegradable materials is to control the degradation rate [5]. The alloying method is widely used to improve the properties of alloys [6–8]. Silver, with the ability to enhance the antibacterial and biocompatibility of alloys, can also improve the mechanical properties of alloys and grain refinement [8,9]. The addition of silver can effectively promote bone formation and the function of osteoblasts while reducing osteoclast activity and bone absorption [10]. It has been reported that a certain amount of Ag as solute atom can improve the corrosion resistance of alloys [11,12]. However, due to the existence of secondary phases, the corrosion rate is still high. It is reported that the addition of Cu leads to grain refinement, which increases the corrosion resistance of magnesium-based alloys [13]. As a trace element in the human body, copper has excellent biocompatibility and antibacterial properties [14]. Several Mg-Cu alloys have been investigated with effective antibacterial

* Corresponding authors.
E-mail addresses: jian.wang@polymtl.ca (J. Wang), lysheng@yeah.net (L. Sheng).

https://doi.org/10.1016/j.jma.2020.12.019

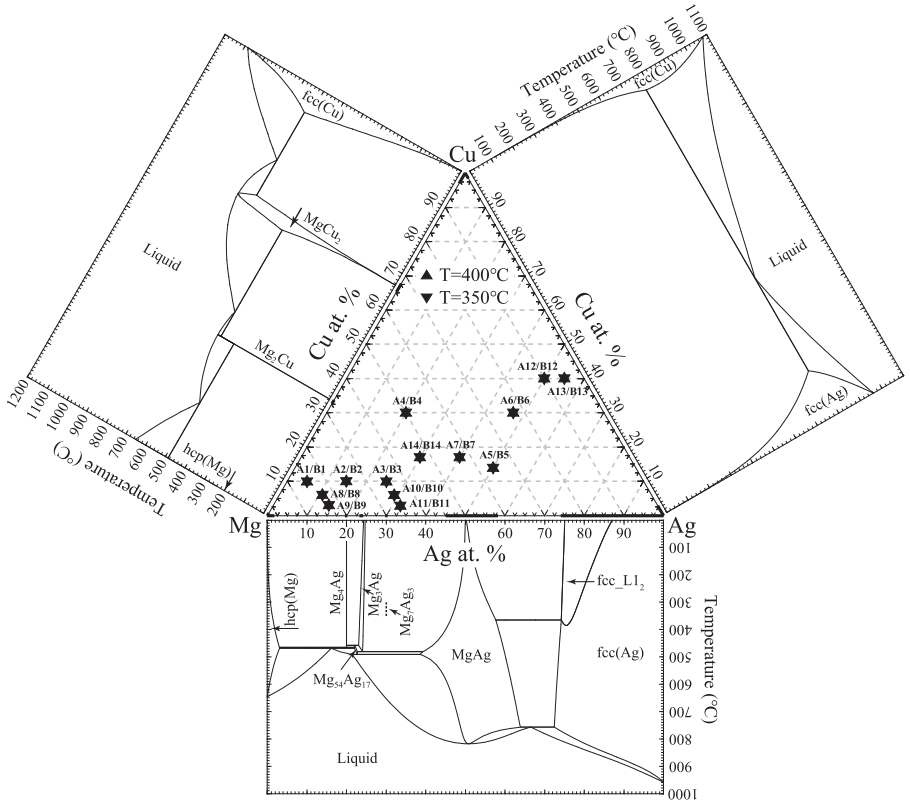

Fig. 1. The phase diagram of the Mg–Ag–Cu ternary system with key alloy compositions selected in the present work.

properties *in vitro* and in vivo [15]. The formation of collagen in bones, blood vessels and skin can be promoted with the addition of copper [14]. Thus, silver and copper are of great potential additive elements for magnesium-based biomaterials development. The Mg–Ag–Cu ternary alloys selected as a promising materials for biodegradable implants development, it is necessary to have a thorough knowledge of the phase equilibria, which is the "guide map" to understand the relationships among the microstructures, mechanical properties and biological properties of new designed alloys. To the best of our knowledge, there are few experimental data available for the Mg–Ag–Cu ternary system. Therefore, a thorough study of the Mg–Ag–Cu ternary phase equilibria is of great importance for magnesium-based biomaterials development.

The phase diagrams of three binary subsystems of the Mg–Ag–Cu ternary system: Mg–Ag [16–21], Mg–Cu [22–26] and Ag–Cu [27] have been investigated previously with experimental and thermodynamic modeling methods. The accepted phase diagrams are shown in Fig. 1, which are used in the present work. Seven phases hcp(Mg), Mg_4Ag, Mg_3Ag, Mg_7Ag_3, MgAg, fcc_$L1_2$ and fcc(Ag) are reported in the Mg–Ag binary system. The fcc_$L1_2$ phase is the ordered phase of the fcc(Ag). The fcc(Ag) phase has the maximum solid solubility of 28 at.% Mg at about 760 °C. The maximum solid solubility range of the intermetallic compound MgAg (Bcc_B2) was reported to be 39 at.% to 64 at.% Ag. The compound Mg_3Ag has a solid solubility range of about 1 at.%. Recently, an intermetallic phase Mg_7Ag_3 was reported at temperature of 300 and 350 °C by the diffusion couple and equilibrated alloy methods [21,28]. The crystal structure of the Mg_7Ag_3 phase was also identified, and the profile of Mg_7Ag_3 phase was found to be very similar to that of $Mg_{51}Zn_{20}$ [21]. The phase diagram of Mg-Cu binary system is constituted with two terminal solutions hcp(Mg), fcc(Cu) and two intermetallic compounds Mg_2Cu and $MgCu_2$. The solid solubility of compound $MgCu_2$ was reported to be 64.2 to 67.9 at.% Cu at 550 °C. The solubility of Mg in fcc was reported to be about 7 at.% at 772 °C [26]. The Ag–Cu binary system is constituted with a simple eutectic type liquid ↔ fcc(Ag) + fcc(Cu). The solid solubility limit of Cu in fcc(Ag) was reported to be about 14 at.% at 780 °C. The solid solubility limit of Ag in fcc (Cu) was reported to be less than 5 at.% above the eutectic temperature. All the solid phases and their crystal structure information of the Mg–Ag–Cu ternary system are summarized in Table 1.

The main purpose of the present work is to investigate the isothermal sections of the Mg–Ag–Cu ternary system at 350 and 400 °C using the equilibrated alloy method. This work is a part of a comprehensive research program to develop a thermodynamic database of Mg-X (X: Zn, Ag, Ca, Cu, Sr, Y) based alloys for biomaterials development [7,8,29–31].

2. Materials and methods

The phase equilibria of the Mg–Ag–Cu ternary system were predicted according to the calculations with the

Table 1
Crystallographic information on the solid phases of the Mg–Ag–Cu ternary system.

System	Phase	Pearson symbol	Strukturbericht designation	Space group	Prototype
Mg–Ag	hcp(Mg)	hP2	A3	$P6_3/mmc$	Mg
	fcc(Ag)	cF4	A1	$Fm\bar{3}m$	Cu
	fcc_$L1_2$	cP4	$L1_2$	$Pm\bar{3}m$	$AuCu_3$
	MgAg	cP2	B2	$Pm\bar{3}m$	CsCl
	Mg_3Ag	cF264	–	$Fm\bar{3}$	$Mg_{26}Ag_7$
	Mg_4Ag	hP92	–	$P6_3$	$Mg_{37}Ag_9$
	Mg_7Ag_3	–	–	Immm	–
	$Mg_{54}Ag_{17}$	oI142	–	Immm	$Mg_{54}Ag_{17}$
Mg-Cu	hcp(Mg)	hP2	A3	$P6_3/mmc$	Mg
	fcc(Cu)	cF4	A1	$Fm\bar{3}m$	Cu
	Mg_2Cu	oF48	C_b	Fddd	Mg_2Cu
	$MgCu_2$	cF24	C15	Fd-3m	$MgCu_2$
Ag–Cu	fcc(Ag)	cF4	A1	$Fm\bar{3}m$	Cu
	fcc(Cu)	cF4	A1	$Fm\bar{3}m$	Cu

thermodynamic database of the Mg–Ag, Mg–Cu and Ag–Cu binary systems. Fourteen key alloys (A1-A7, B1-B7) were selected for the first time based on the calculation results in order to obtain a universal information of phase equilibria relationship of the Mg–Ag–Cu ternary system at 350 and 400 °C. Then, other fourteen key samples (A8-A14, B8-B14) were supplemented to construct the whole phase equilibria relationship of the Mg–Ag–Cu ternary system. To summary, twenty-eight ternary key samples of the Mg–Ag–Cu ternary system were prepared using pure magnesium (99.9 wt.%), silver (99.95 wt.%), and copper (99.9 wt.%) purchased from Trillion Metals company, Beijing, China. The compositions of key samples used in the present work are shown in Fig. 1 and listed in Table 2.

All raw materials were stored separately in dry bottles. Cylindrical graphite crucibles were used to avoid the reaction between the sample and the crucible. All samples were melted at least twice in an induction furnace under the argon atmosphere to obtain the homogeneous microstructure. The weight loss in the melting process was controlled within 2%, which is mainly due to the volatilization of magnesium. All as-cast samples were sealed into quartz tubes and were annealed at 350 °C for 35 days and 400 °C for 28 days in a tubular furnace. Precautions were taken to avoid undesirable reactions, such as vacuum-seal the samples into quartz tubes and quenching without breaking the quartz tubes in the water. Then, all samples were ground with 400, 800, 1000 and 2000 grit particle sizes of abrasive paper and polished with 99.7% pure methanol as a lubricant. After polishing, samples were washed in 99.9% pure ethanol for 30 s by ultrasonic machine to remove the polishing paste and impurities remained on the sample surface. Polished samples were sealed in a plastic vacuum bag by vacuum sealing device to prevent oxidation.

Gemini SEM 300 scanning electron microscopy (SEM) equipped with an energy-dispersive spectroscopy (EDS) was used to analyze the phase assemblage and compositions of all samples. An accelerating voltage of 15 kV was employed with a maximum spot size of 3 μm and counting times of 60 s. The phase composition was averaged from five reliable data obtained from EDS. The standard deviation is within 1 at.%.

The powder X-ray diffraction technique (XRD) was performed to identify the crystal structures of phases in annealed key samples. During the grinding procedure, a small amount of paraffin oil was added to reduce oxidation. The spectra were acquired from 20° to 90° (2θ) with a 0.1 step size. The X-ray patterns were obtained by D8 advance polycrystalline machine with the 45 kV and 40 mA CuKα radiation. The XRD patterns were analyzed using the Jade6 analysis software and Pearson's crystal database.

3. Results and discussion

The phase equilibria of the Mg–Ag–Cu ternary system at 350 and 400 °C obtained in the present work are shown in Fig. 2a,b.

3.1. The isothermal section of the Mg–Ag–Cu ternary system at 350 °C

The isothermal section of the Mg–Ag–Cu ternary system at 350 °C is presented in Fig. 2a. The BSD image of the sample A1 as shown in Fig. 3a suggests a three-phase equilibrium of hcp(Mg) + Mg_2Cu + Mg_3Ag (or Mg_4Ag). Since the difference of compositions between the compounds Mg_4Ag and Mg_3Ag is rather small, the XRD technique was carried out on sample A1 to identify the phase constitution. The X-ray diffraction result of sample A1 is shown in Fig. 4a. Based on the analysis results of the XRD patterns, the phase equilibrium of sample A1 was confirmed to be hcp(Mg) + Mg_2Cu + Mg_3Ag. It was observed a three-phase equilibrium of Mg_2Cu + Mg_3Ag + MgAg in the sample A3. Another three-phase equilibrium Mg_2Cu + $MgCu_2$ + MgAg was observed in the samples A4 and A14. The BSD images of the samples A3 and A4 are shown in Fig. 3b,c, and their phase constitutions Mg_2Cu + Mg_3Ag + MgAg and Mg_2Cu + $MgCu_2$ + MgAg were confirmed by the XRD results as shown in Fig. 4b-c. Two three-phase equilibria

Table 2
Equilibrium compositions obtained from key samples of the Mg–Ag–Cu ternary system at 350 and 400 °C (Continued).

Isothermal section	Alloy No.	Alloy nominal composition (at.%)	Alloy actual composition (at.%)	Phase equilibria Phase 1/Phase 2/Phase 3	Composition determined by EDS (at.%)								
					Phase 1			Phase 2			Phase 3		
					Mg	Ag	Cu	Mg	Ag	Cu	Mg	Ag	Cu
350 °C	A1	Mg85Ag5Cu10	Mg86.6Ag4.9Cu8.5	hcp(Mg)/Mg_2Cu/Mg_3Ag	99.57	0.42	0.01	64.84	1.65	33.51	71.29	15.18	13.53
	A2	Mg75Ag15Cu10	Mg73.9Ag15.5Cu10.6	hcp(Mg)/Mg_3Ag	97.85	1.51	0.64	71.07	17.17	11.76	–	–	–
	A3	Mg65Ag25Cu10	Mg62.5Ag24.3Cu13.2	Mg_2Cu/Mg_3Ag/MgAg	65.04	4.45	30.51	68.66	20.88	10.46	48.39	44.92	6.69
	A4	Mg50Ag20Cu30	Mg51.3Ag16.9Cu31.8	Mg_2Cu/$MgCu_2$/MgAg	63.63	3.51	32.86	33.90	0.77	65.33	44.92	42.34	12.74
	A5	Mg36Ag50Cu14	Mg32.1Ag47.8Cu20.1	$MgCu_2$/MgAg/fcc_$L1_2$	24.71	9.57	65.72	36.59	57.22	6.19	24.31	70.30	5.39
	A6	Mg23Ag47Cu30	Mg19.7Ag42.6Cu37.7	$MgCu_2$/fcc_$L1_2$/fcc(Cu)	23.21	11.46	65.33	22.57	66.23	11.20	3.88	1.33	94.79
	A7	Mg43Ag40Cu17	Mg38.5Ag38.6Cu22.9	$MgCu_2$/MgAg	29.24	5.50	65.26	42.10	49.48	8.42	–	–	–
	A8	Mg83Ag11Cu6	Mg83.1Ag11.3Cu5.6	hcp(Mg)/Mg_3Ag	98.35	1.35	0.30	71.32	18.31	10.37	–	–	–
	A9	Mg83Ag14Cu3	Mg83.3Ag13.7Cu3.0	hcp(Mg)/Mg_3Ag	99.17	0.83	0.00	72.39	21.97	5.64	–	–	–
	A10	Mg65Ag29Cu6	Mg63.6Ag28.5Cu7.9	Mg_3Ag/MgAg	69.31	21.68	9.01	49.99	46.20	3.81	–	–	–
	A11	Mg65Ag32Cu3	Mg64.0Ag32.1Cu3.9	Mg_3Ag/MgAg	69.46	25.27	5.27	50.91	48.21	0.88	–	–	–
	A12	Mg10Ag50Cu40	Mg8.7Ag48.5Cu42.8	fcc(Ag)/fcc(Cu)	13.18	73.70	13.12	0.36	3.56	96.08	–	–	–
	A13	Mg5Ag55Cu40	Mg4.3Ag49.9Cu45.8	fcc(Ag)/fcc(Cu)	7.25	77.63	15.12	0.49	4.30	95.21	–	–	–
	A14	Mg53Ag30Cu17	Mg51.5Ag28.2Cu20.3	Mg_2Cu/$MgCu_2$/MgAg	64.50	3.30	32.20	33.93	0.97	65.10	46.09	40.47	13.44
400 °C	B1	Mg85Ag5Cu10	Mg86.6Ag4.9Cu8.5	hcp(Mg)/Mg_2Cu/Mg_3Ag	98.49	0.78	0.73	66.22	1.84	31.94	72.11	13.08	14.81
	B2	Mg75Ag15Cu10	Mg73.9Ag15.5Cu10.6	hcp(Mg)/Mg_3Ag	99.00	0.12	0.88	72.39	16.07	11.54	–	–	–
	B3	Mg65Ag25Cu10	Mg62.5Ag24.3Cu13.2	Mg_2Cu/Mg_3Ag/MgAg	64.87	5.11	30.02	68.64	20.39	10.97	49.10	43.01	7.89
	B4	Mg50Ag20Cu30	Mg51.3Ag16.9Cu31.8	Mg_2Cu/$MgCu_2$/MgAg	63.51	3.85	32.64	33.00	1.71	65.29	45.82	37.96	16.22
	B5	Mg36Ag50Cu14	Mg32.1Ag47.8Cu20.1	$MgCu_2$/MgAg/fcc(Ag)	24.44	9.58	65.98	36.19	61.34	2.47	23.04	73.00	3.96
	B6	Mg23Ag47Cu30	Mg19.7Ag42.6Cu37.7	$MgCu_2$/fcc(Ag)/fcc(Cu)	23.74	11.25	65.01	20.72	66.92	12.36	2.90	1.21	95.89
	B7	Mg43Ag40Cu17	Mg38.5Ag38.6Cu22.9	$MgCu_2$/MgAg	29.16	5.00	65.84	42.48	51.11	6.41	–	–	–
	B8	Mg83Ag11Cu6	Mg83.1Ag11.3Cu5.6	hcp(Mg)/Mg_3Ag	98.49	1.51	0.00	72.88	16.75	10.37	–	–	–
	B9	Mg83Ag14Cu3	Mg83.3Ag13.7Cu3.0	hcp(Mg)/Mg_3Ag	97.49	2.50	0.01	72.88	21.64	5.48	–	–	–
	B10	Mg65Ag29Cu6	Mg63.6Ag28.5Cu7.9	Mg_3Ag/MgAg	68.80	22.49	8.71	50.97	44.60	4.43	–	–	–
	B11	Mg65Ag32Cu3	Mg64.0Ag32.1Cu3.9	Mg_3Ag/MgAg	69.84	24.78	5.38	53.82	44.77	1.41	–	–	–
	B12	Mg10Ag50Cu40	Mg8.7Ag48.5Cu42.8	fcc(Ag)/fcc(Cu)	13.24	74.42	12.34	0.50	3.68	95.82	–	–	–
	B13	Mg5Ag55Cu40	Mg4.3Ag49.9Cu45.8	fcc(Ag)/fcc(Cu)	7.93	79.21	12.86	0.26	4.51	95.23	–	–	–
	B14	Mg53Ag30Cu17	Mg51.5Ag28.2Cu20.3	Mg_2Cu/MgAg	63.95	4.34	31.71	46.23	37.61	16.16	–	–	–

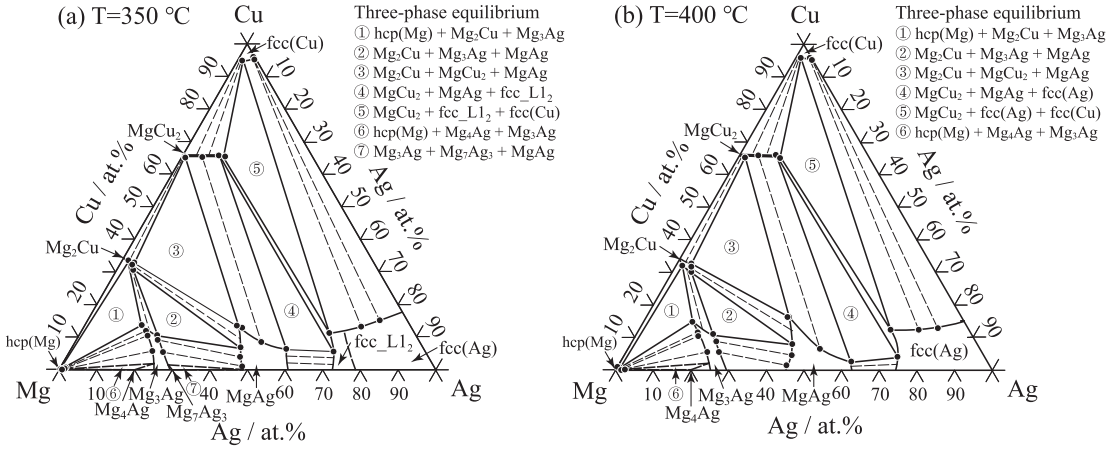

Fig. 2. Isothermal sections of the Mg–Ag–Cu system at 350 and 400 °C obtained in the present work.

$MgCu_2 + MgAg + fcc\_L1_2$ and $MgCu_2 + fcc\_L1_2 + fcc(Cu)$ were observed in samples A5 and A6, respectively. The phase constitutions indicated in the BSD images of the samples A5 and A6 (see Fig. 3d,e) were confirm by the XRD results. Because of the high hardness of samples A5 and A6 located in the Cu-rich and Ag-rich region, the particle size of samples grinded for the XRD test was a bit large, which results in the weak intensity of the diffraction peaks (see Fig. 5). According to the SEM/EDS and XRD results, the phase equilibria of $MgCu_2 + MgAg + fcc\_L1_2$ and $MgCu_2 + fcc\_L1_2 + fcc(Cu)$ were confirmed. As shown in the Mg–Ag binary system (see Fig. 1), a secondary phase transition of fcc(Ag) and fcc_L1_2 was reported in the Ag-rich region. The fcc_L1_2 phase is the ordered phase of fcc(Ag). But, the diffraction peaks of fcc(Ag) and fcc_L1_2 are extremely similar as shown in Fig. 5, which is hard to

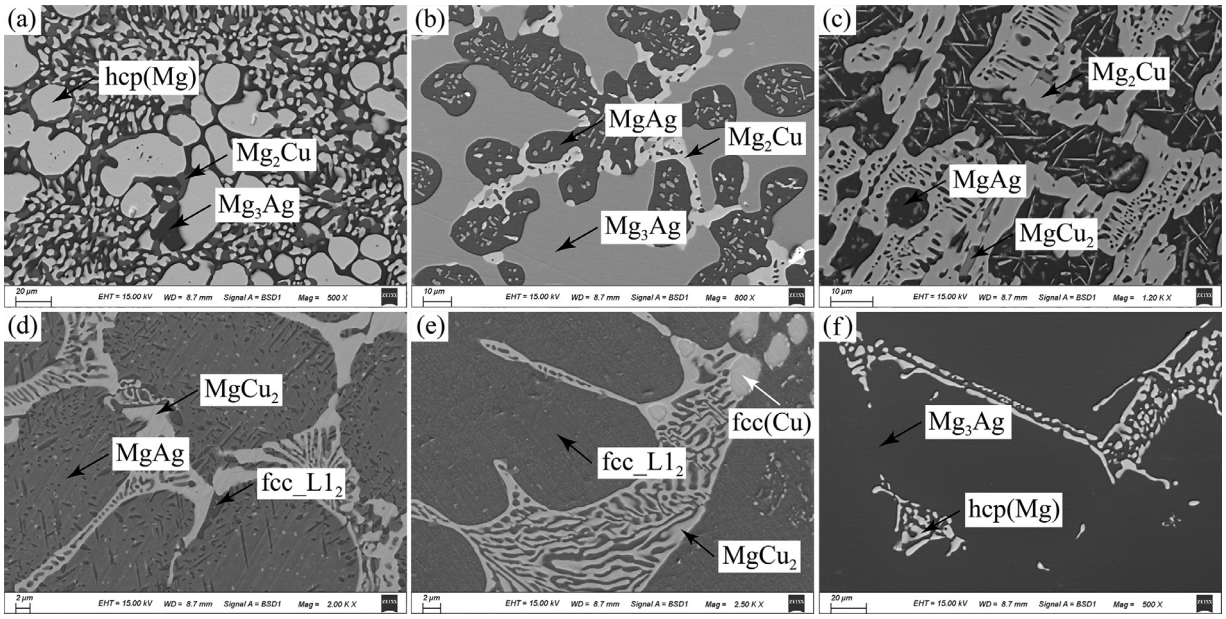

Fig. 3. The BSD images obtained from key samples: (a) A1 ($Mg_{85}Ag_5Cu_{10}$), (b) A3 ($Mg_{65}Ag_{25}Cu_{10}$), (c) A4 ($Mg_{50}Ag_{20}Cu_{30}$), (d) A5 ($Mg_{36}Ag_{50}Cu_{14}$), (e) A6 ($Mg_{23}Ag_{47}Cu_{30}$), (f) A2 ($Mg_{75}Ag_{15}Cu_{10}$) annealed at 350 °C for 35 days.

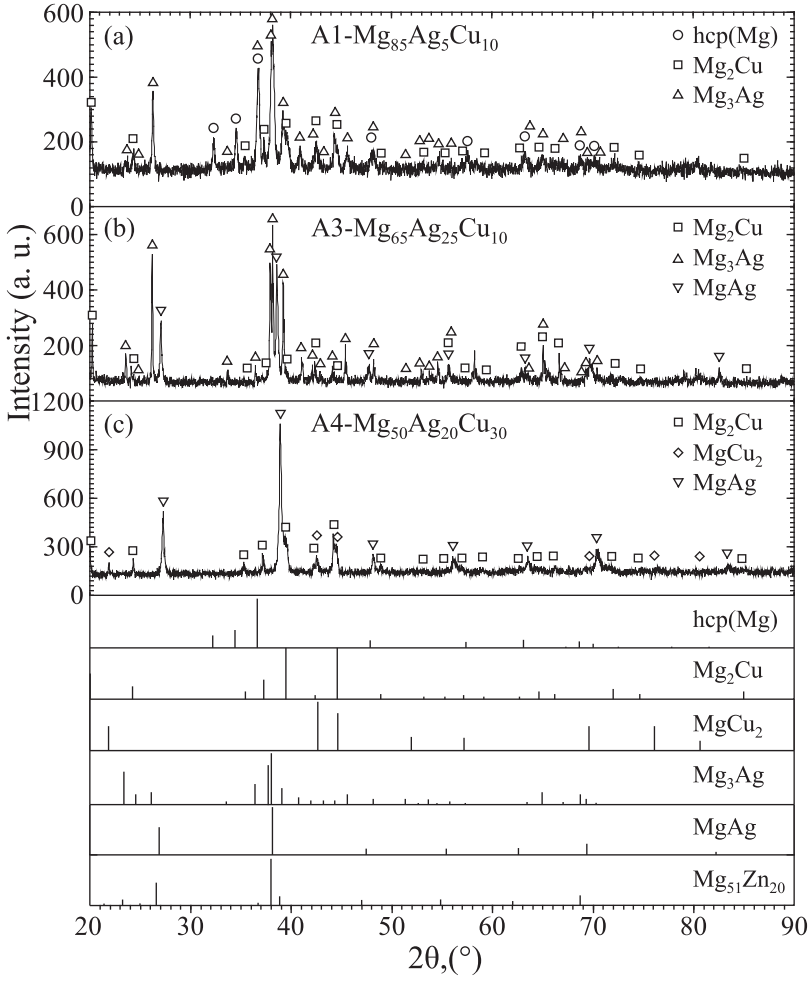

Fig. 4. The XRD patterns obtained from key samples: (a) A1 ($Mg_{85}Ag_5Cu_{10}$), (b) A3 ($Mg_{65}Ag_{25}Cu_{10}$), (c) A4 ($Mg_{50}Ag_{20}Cu_{30}$) annealed at 350 °C for 35 days.

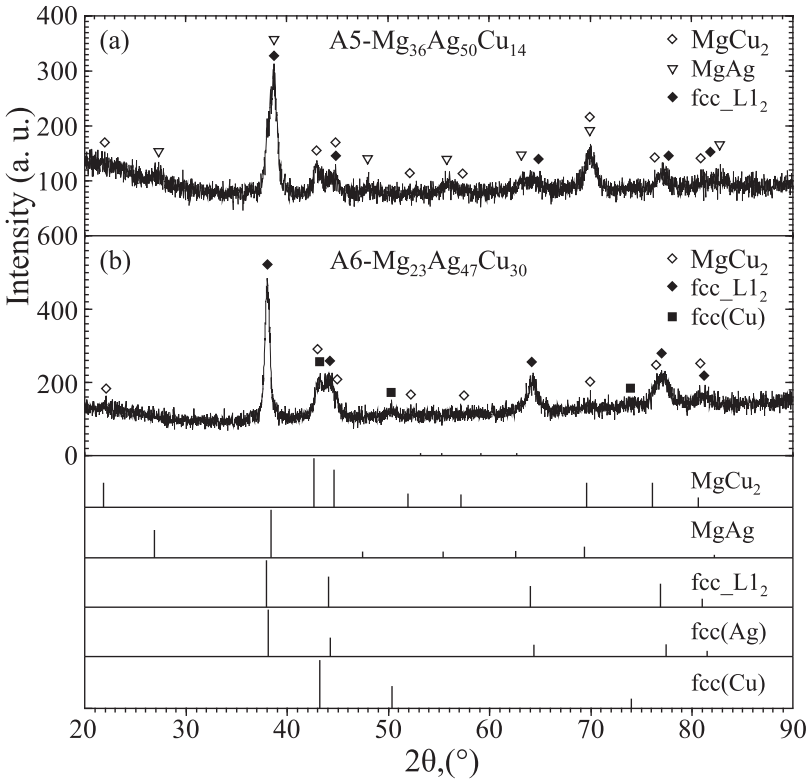

Fig. 5. The XRD patterns obtained from key samples: (a) A5 ($Mg_{36}Ag_{50}Cu_{14}$), (b) A6 ($Mg_{23}Ag_{47}Cu_{30}$) annealed at 350 °C for 35 days.

distinguish between these two phases based on XRD patterns analysis. Thus, in the present work, the phase boundary of fcc(Ag) and fcc_$L1_2$ of Mg–Ag–Cu ternary system was only predicted based on the fcc(Ag)/fcc_$L1_2$ phase boundary of the Mg–Ag binary system.

Besides, several two-phase equilibria regions in the isothermal section of 350 °C were observed by key samples as shown in Fig. 2. Two-phase equilibrium of hcp(Mg) + Mg_3Ag was observed in samples A2, A8 and A9, respectively. The BSD images of sample A2 is shown in Fig. 3f. Two-phase equilibrium of Mg_3Ag + MgAg was obtained in samples A10 and A11. A two-phase equilibrium of $MgCu_2$ + MgAg was observed in sample A7. A two-phase equilibrium of fcc(Ag) + fcc(Cu) was established in samples A12 and A13. The BSD images of samples A10, A7 and A12 are shown in Fig. 6a-c. According to the Mg–Ag binary phase diagram, the three-phase equilibrium region of hcp(Mg) + Mg_4Ag + Mg_3Ag should exist in the Mg-rich region. Moreover, the three-phase equilibrium region of Mg_3Ag + Mg_7Ag_3 + MgAg should exist at 350 °C in the Mg–Ag–Cu ternary system. However, the three-phase equilibrium regions of hcp(Mg) + Mg_4Ag + Mg_3Ag and Mg_3Ag + Mg_7Ag_3 + MgAg were not observed in the present work. These three-phase equilibrium regions may be too narrow to be measured. Thus, they were predicted based on the present experimental results as shown in Fig. 2.

As listed in Table 2, the EDS results of samples A1, A2, A3, A8, A9, A10 and A11 indicated that the intermetallic compound Mg_3Ag has a large solid solubility range. As seen in Fig. 4a,b, the major diffraction peaks of the compound Mg_3Ag shifted a little to the right. Since the atomic radius of Ag and Cu are a little smaller than the atomic radius of Mg, the substitution of Ag/Cu with Mg decreases of the value of d. This means the diffraction peaks would shift to the right based on the Bragg's formula $2d \cdot \sin\theta = n\lambda$ (d: Lattice parameter, θ: Incident angle, n: Diffraction order, λ: Incident wavelength), which is consistent with our XRD experimental observation. The maximum solid solubility of Cu in the compound Mg_3Ag was determined to be 13.53 at.% at 350 °C.

According to the EDS results of samples A3, A4, A5, A7, A10, A11 and A14, the intermetallic compound MgAg might has a broad solid solubility. The XRD technique was carried out on samples A3, A4, A5 and A6 to investigate the solid solubility of the compound MgAg. The XRD patterns of samples A3, A4 and A5 are shown in Fig 4b,c and Fig 5a, respectively. The major diffraction peaks of the compound MgAg shifted to the right (see Figs. 4 and 5). The EDS results indicated that the solid solubility is mainly caused by the substitution of Ag/Cu with Mg. These results are in good agreement based on the discussion mentioned above. The maximum solid solubility of Cu in the compound MgAg was determined to be 12.74 at.% at 350 °C.

As shown in Fig. 2a, the intermetallic compound $MgCu_2$ has a solid solubility, which might be due to the substitution of Ag with Mg. The XRD technique was used to investigate the samples A4, A5 and A6 to confirm the solid solubility of the compound $MgCu_2$. The XRD patterns of the samples A4, A5 and A6 are shown in Fig. 4c and Fig. 5a,b. Five

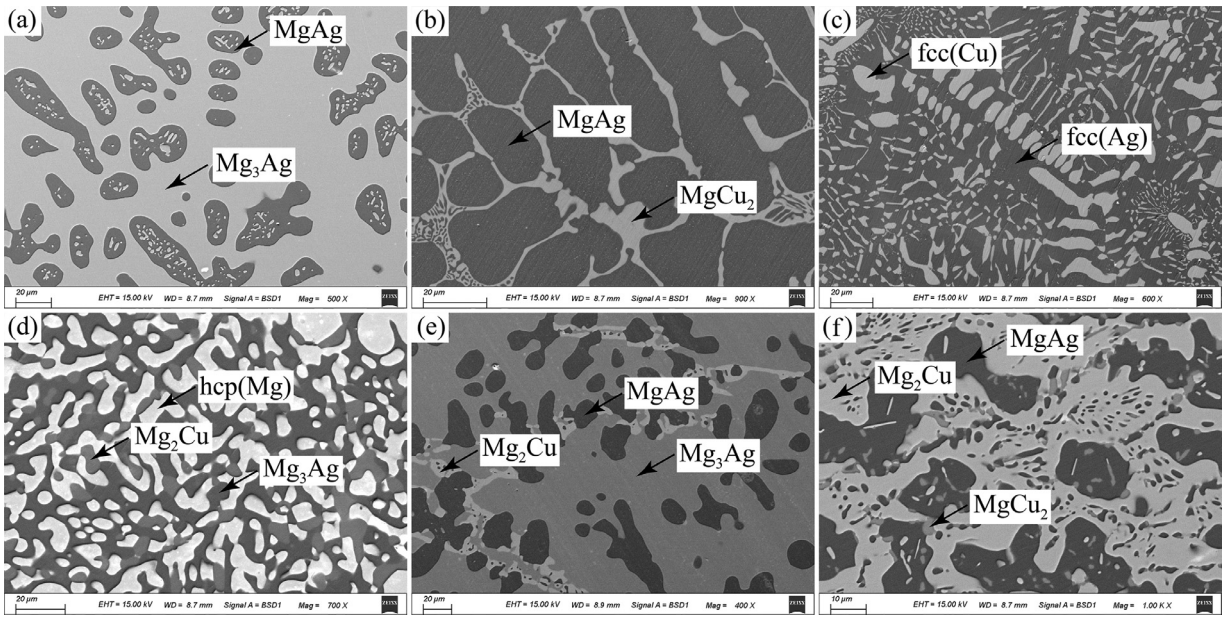

Fig. 6. The BSD images obtained from key samples: (a) A10 ($Mg_{65}Cu_{29}Sr_6$), (b) A7 ($Mg_{43}Cu_{40}Sr_{17}$), (c) A12 ($Mg_{10}Cu_{50}Sr_{40}$) annealed at 350 °C for 35 days and (d) B1 ($Mg_{85}Ag_5Cu_{10}$), (e) B3 ($Mg_{65}Ag_{25}Cu_{10}$), (f) B4 ($Mg_{50}Ag_{20}Cu_{30}$) annealed at 400 °C for 28 days.

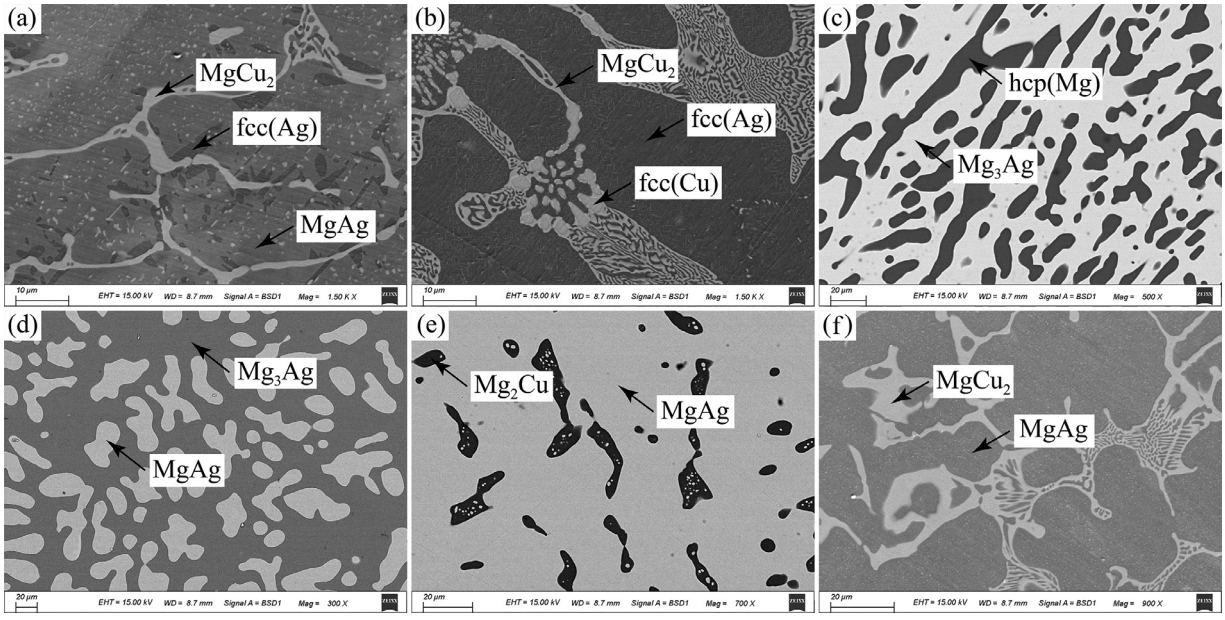

Fig. 7. The BSD images obtained from key samples: (a) B5 ($Mg_{36}Ag_{50}Cu_{14}$), (b) B6 ($Mg_{23}Ag_{47}Cu_{30}$), (c) B8 ($Mg_{83}Ag_{11}Cu_6$), (d) B11 ($Mg_{65}Ag_{32}Cu_3$), (e) B14 ($Mg_{53}Ag_{30}Cu_{17}$), (f) B7 ($Mg_{43}Ag_{40}Cu_{17}$) annealed at 400 °C for 28 days.

peaks assigned to the $MgCu_2$ phase gradually shift to the right with the increase of Ag in the samples A4, A5 and A6. As discussed above, since the atomic radius of Ag is smaller than that of Mg, the substitution of Ag with Mg would decrease the value of d which results in the right shifting of the diffraction peaks. The XRD results of samples A4, A5 and A6 are in good agreement with the EDS analysis. The maximum solid solubility of Ag in the compound $MgCu_2$ was measured to be 11.46 at.% with a constant value of 66 at.% Cu at 350 °C.

According to the EDS results of the fcc_$L1_2$ (or fcc(Ag)) phase observed in samples A5, A6, A12 and A13, the solid solubility range of fcc_$L1_2$ (or fcc(Ag)) was presented in Fig. 2a. As demonstrated in Fig. 5a, the diffraction peaks of fcc_$L1_2$ phase in the sample A5 shifted 0.5° to the right. As shown in Fig. 5b, the diffraction peaks of fcc_$L1_2$ phase in sample A6 is almost the same as the standard. Because the atomic radius of Ag is between Mg and Cu, it is reasonable that the diffraction peaks of fcc_$L1_2$ phase in samples A5 and A6 have an offset. The maximum solid solubility of Mg

in the terminal solution fcc_$L1_2$ (or fcc(Ag)) was determined to be 24.71 at.% at 350 °C. In addition, the solid solubility limits of Ag in the compounds Mg_2Cu and fcc(Cu) were less than 5 at.% at 350 °C.

3.2. The isothermal section of the Mg–Ag–Cu ternary system at 400 °C

The isothermal section of the Mg–Ag–Cu ternary system at 400 °C is shown in Fig. 2b. The three-phase equilibrium of hcp(Mg) + Mg_2Cu + Mg_3Ag was observed in the sample B1 as shown in Fig. 6d. Another three-phase equilibrium of Mg_2Cu + Mg_3Ag + MgAg was identified in the sample B3 as shown in Fig. 6e. A three-phase equilibrium Mg_2Cu + $MgCu_2$ + MgAg was obtained in the sample B4 as shown in Fig. 6f. The BSD images of the samples B5 and B6 are presented in Fig. 7a,b, two three-phase equilibrium assemblages of $MgCu_2$ + MgAg + fcc(Ag) and $MgCu_2$ + fcc(Ag) + fcc(Cu) were observed in the samples B5 and B6, respectively. The BSD images of the samples B8 and B11 are shown in Fig. 7c,d. The two-phase equilibrium of hcp(Mg) + Mg_3Ag was observed in the samples B2, B8 and B9. The BSD images of the samples B14 and B7 are presented in Fig. 7e–f. The two-phase equilibrium of Mg_3Ag + MgAg was observed in the samples B10 and B11. A two-phase equilibrium of Mg_2Cu + MgAg was observed in the sample B14. A two-phase equilibrium of $MgCu_2$ + MgAg was observed in the sample B7. A two-phase equilibrium of fcc(Ag) + fcc(Cu) was observed in the samples B12 and B13.

The maximum solid solubility of Cu in the compound Mg_3Ag was measured to be 14.81 at.% at 400 °C, which is 1.28 at.% higher than that obtained at 350 °C. The maximum solid solubility of Cu in the compound MgAg was determined to be 16.22 at.% at 400 °C, which is 3.48 at.% higher than that obtained at 350 °C. The maximum solid solubility of Ag in the compound $MgCu_2$ was found to be 11.25 at.% with a constant value of about 66 at.% Cu at 400 °C, which is almost the same as that obtained at 350 °C. The maximum solid solubility of Mg in the terminal solution fcc(Ag) was measured to be 20.72 at.% at 400 °C. Besides, the solid solubility limits of Ag in the compounds Mg_2Cu and fcc(Cu) were measured to be less than 5 at.% at 400 °C.

4. Conclusions

The Mg–Ag–Cu ternary phase equilibria at 350 and 400 °C were experimentally established using key samples method with SEM/EDS and XRD techniques. Five three-phase equilibrium regions: hcp(Mg) + Mg_2Cu + Mg_3Ag, Mg_2Cu + Mg_3Ag + MgAg, Mg_2Cu + $MgCu_2$ + MgAg, $MgCu_2$ + MgAg + fcc_$L1_2$ and $MgCu_2$ + fcc_$L1_2$ + fcc(Cu) have been identified and confirmed at 350 °C. Five three-phase equilibrium regions: hcp(Mg) + Mg_2Cu + Mg_3Ag, Mg_2Cu + Mg_3Ag + MgAg, Mg_2Cu + $MgCu_2$ + MgAg, $MgCu_2$ + MgAg + fcc(Ag) and $MgCu_2$ + fcc(Ag) + fcc(Cu) have been identified and confirmed at 400 °C. The maximum solid solubility of Cu in the compound Mg_3Ag was determined to be 13.53 at.% at 350 °C. The maximum solid solubility of Cu in the compound MgAg was determined to be 12.74 at.% at 350 °C. The maximum solid solubility of Ag in the compound $MgCu_2$ was determined to be 11.46 at.% at a constant value of about 66 at.% Cu at 350 °C. The maximum solid solubility of Mg in the terminal solution fcc_$L1_2$ (or fcc(Ag)) was determined to be 24.71 at.% at 350 °C. The maximum solid solubility of Cu in the compound Mg_3Ag was determined to be 14.81 at.% at 400 °C. The maximum solid solubility of Cu in the compound MgAg was determined to be 16.22 at.% at 400 °C. The maximum solid solubility of Ag in the compound $MgCu_2$ was determined to be 11.25 at.% at a constant value of about 66 at.% Cu at 400 °C. The maximum solid solubility of Mg in the terminal solution fcc(Ag) was determined to be 20.72 at.% at 400 °C. In addition, the solid solubility limits of the compounds Mg_2Cu and fcc(Cu) were less than 5 at.% at 350 and 400 °C.

Declaration of Competing Interest

Author Jian Wang has received research grant from the Science and Technology Project of Shenzhen city. This manuscript is approved by all authors for publication. I would like to declare on behalf of my co-authors that the work described was original research that has not been published previously, and have no conflict of interest.

Acknowledgment

Financial supports from the Science and Technology Project of Shenzhen city (No. JCYJ20170815153210359) are gratefully acknowledged.

References

[1] Chen QZ, G.A. Thouas, Metallic implant biomaterials, Mater. Sci. Eng. R 87 (2015) 1–57.
[2] J.J. Han, P. Wan, Y. Ge, X.M. Fan, L.L. Tan, J.J. Li, K. Yang, Tailoring the degradation and biological response of a magnesium-strontium alloy for potential bone substitute application, Mater. Sci. Eng. C 58 (2016) 799–811.
[3] N. Sezer, Z. Evis, S.M. Kayhan, A. Tahmasebifar, M. Koc, Review of magnesium-based biomaterials and their applications, J. Magnes. Alloy 6 (2018) 23–43.
[4] S. Agarwal, J. Curtin, B. Duffy, S. Jaiswal, Biodegradable magnesium alloys for orthopaedic applications: a review on corrosion, biocompatibility and surface modifications, Mater. Sci. Eng. C 68 (2016) 948–963.
[5] G. Song, Control of biodegradation of biocompatable magnesium alloys, Corros. Sci. 49 (2007) 1696–1701.
[6] Z. Zhang, Q. Zhang, L.L. Jin, et al., Experimental determination of the phase equilibrium in the Mg–Cu–Ca ternary system at 350 °C, J. Alloys Compd. 2,019, (2019) 152,865.
[7] J. Wang, Y.N. Zhang, P. Hudon, P. Chartrand, I.-.H. Jung, M. Medraj, Experimental determination of the phase equilibria in the Mg–Zn–Sr ternary system, J. Mater. Sci. 50 (2015) 7636–7646.
[8] J. Wang, Y.N. Zhang, P. Hudon, I.-.H. Jung, M. Medraj, P. Chartrand, Experimental study of the phase equilibria in the Mg–Zn–Ag ternary system at 300 °C, J. Alloy Compd. 639 (2015) 593–601.
[9] X.B. Zhang, Z.X. Ba, Z.Z. Wang, H.C. He, C. Shen, Q. Wang, Influence of silver addition on microstructure and corrosion behavior of Mg–Nd–Zn–Zr alloys for biomedical application, Mater. Lett. 100 (2013) 188–191.

[10] K. Jähn, H. Saito, H. Taipaleenmäki, et al., Intramedullary Mg_2Ag nails augment callus formation during fracture healing in mice, Acta Biomater. 36 (2016) 350–360.
[11] L.Q. Wang, G.W. Qin, S.N. Sun, Y.P. Ren, S. Li, Effect of solid solution treatment on *in vitro* degradation rate of as-extruded Mg–Zn–Ag alloys, T Nonferr. Metal Soc. 27 (2017) 2607–2612.
[12] G. Ben-Hamu, D. Eliezer, A. Kaya, Y.G. Na, K.S. Shin, Microstructure and corrosion behavior of Mg–Zn–Ag alloys, Mater. Sci. Eng. A 435-436 (2006) 579–587.
[13] R. Xu, M.C. Zhao, Y.C. Zhao, et al., Improved biodegradation resistance by grain refinement of novel antibacterial ZK30-Cu alloys produced via selective laser melting, Mater. Lett. 237 (2019) 253–257.
[14] S.J. Jin, L. Ren, K. Yang, Bio-functional Cu containing biomaterials: a new way to enhance bio-adaption of biomaterials, J. Mater. Sci. Technol. 32 (2016) 835–839.
[15] Y. Li, L.N. Liu, P. Wan, et al., Biodegradable Mg-Cu alloy implants with antibacterial activity for the treatment of osteomyelitis: *in vitro* and in vivo evaluations, Biomaterials 106 (2016) 250–263.
[16] J. Wang, P. Hudon, D. Kevorkov, P. Chartrand, I.-.H. Jung, M. Medraj, Thermodynamic and experimental study of the Mg–Sn–Ag–In quaternary system, J Phase Equilib Diff 35 (2014) 284–313.
[17] M. Lim, J.E. Tibballs, P.L. Rossiter, Thermodynamic assessment of Ag–Mg binary system, Z Metallkd 88 (1997) 160–167.
[18] V.E. Kolesnichenko, V.V. Karonik, S.N. Tsyganova, T.A. Kupriyanova, L.N. Sysoeva, Phase equilibria in the Mg–Ag system in the ETA phase region, Izv Akad Nauk SSSR Neorg. Mater. 5 (1988) 186–191.
[19] A.A. Nayeb-Hashemi, J.B. Clark, The Ag–Mg System, Bull. Alloy Phase Diagrams 5 (1984) 348–354.
[20] M.V. Prokofev, V.E. Kolesnichenko, V.V. Karonik, Composition and structure of magnesium-silver alloys with composition near Mg_3Ag, Izv Akad Nauk SSSR Neorg. Mater. 21 (1985) 1332–1334.
[21] Y.P. Ren, H. Zhao, L.Q. Wang, et al., Evidence of a novel intermetallic Mg_7Ag_3 phase in Mg–Ag binary alloy system, J. Appl. Crystallogr. 51 (2018) 844–848.
[22] M. Hämäläinen, N. Bochvar, L.L. Rokhlin, K. Zeng, Thermodynamic evaluation of the Cu–Mg–Zr system, J. Alloy Compd. 285 (1999) 162–166.
[23] M. Mezbahul-Islam, D. Kevorkov, M. Medraj, The equilibrium phase diagram of the magnesium–copper–yttrium system, J. Chem. Thermodyn. 40 (2008) 1064–1076.
[24] W. Xiong, Y. Du, W.W. Zhang, W.H. Sun, X.G. Lu, F.S. Pan, Thermodynamic reassessment of the Cu–Mg–Ni system with brief comments on the thermodynamic modeling of the sub-systems, Calphad 32 (2008) 675–685.
[25] J. Zhao, J. Zhou, S. Liu, Y. Du, S. Tang, Y. Yang, Phase diagram determination and thermodynamic modeling of the Cu–Mg–Si system, J. Min. Metall. B-Metall. 52 (2016) 99–112.
[26] D.L. Cui, I.-.H. Jung, Thermodynamic modeling of the quaternary Al–Cu–Mg–Si system, Calphad 57 (2017) 1–27.
[27] P.R. Subramanian, J.H. Perepezko, The Ag–Cu (silver-copper) system, J. Phase Equilib. 14 (1993) 62–75.
[28] Hong Zhao, Bo Yang, Yuping Ren, G. Qin, Experimental evidence of the $Mg_7(Zn, Ag)_3$ continuous solid solution in Mg-rich corner of Mg–Zn–Ag ternary system at 335 °C, J. Alloy Compd. 789 (2019) 991–995.
[29] Wang J., Han J.J., Du B.N. et al. (2017) Experimental and thermodynamic study of the Mg-Sn-Ca-Sr quaternary system: Part I-Mg–Sn–Ca ternary system, Calphad 58: 6–16.
[30] J. Wang, Y.N. Zhang, P. Hudon, I.-.H. Jung, P. Chartrand, M. Medraj, Experimental study of the crystal structure of the $Mg_{15-x}Zn_xSr_3$ ternary solid solution in the Mg–Zn–Sr system at 300 °C, Mater. Design 86 (2015) 305–312.
[31] J. Wang, Z. Zhang, Y.N. Zhang, et al., Investigation on metallic glass formation in Mg–Zn–Sr ternary system combined with the Calphad, Mater. Lett. 256 (2019) 126628.